



**HAL**  
open science

## Highly-efficient electrochemical label-free immunosensor for the detection of ochratoxin A in coffee samples

Kwanele Kunene, Matthieu Weber, Myalowenkosi Sabela, Damien Voiry, Suvadhan Kanchi, Krishna Bisetty, Mikhael Bechelany

► **To cite this version:**

Kwanele Kunene, Matthieu Weber, Myalowenkosi Sabela, Damien Voiry, Suvadhan Kanchi, et al.. Highly-efficient electrochemical label-free immunosensor for the detection of ochratoxin A in coffee samples. *Sensors and Actuators B: Chemical*, 2020, 305, pp.127438. 10.1016/j.snb.2019.127438 . hal-02507525

**HAL Id: hal-02507525**

**<https://hal.umontpellier.fr/hal-02507525>**

Submitted on 31 May 2021

**HAL** is a multi-disciplinary open access archive for the deposit and dissemination of scientific research documents, whether they are published or not. The documents may come from teaching and research institutions in France or abroad, or from public or private research centers.

L'archive ouverte pluridisciplinaire **HAL**, est destinée au dépôt et à la diffusion de documents scientifiques de niveau recherche, publiés ou non, émanant des établissements d'enseignement et de recherche français ou étrangers, des laboratoires publics ou privés.

1  
2  
3  
4  
5  
6  
7  
8  
9  
10  
11  
12  
13  
14  
15  
16  
17  
18  
19  
20  
21  
22  
23  
24  
25  
26  
27

## Highly-efficient electrochemical label-free immunosensor for the detection of ochratoxin A in coffee samples

Kwanele Kunene<sup>a,b</sup>, Matthieu Weber<sup>a</sup>, Myalowenkosi Sabela<sup>b</sup>, Damien Voiry<sup>a</sup>, Suvardhan Kanchi<sup>b</sup>, Krishna Bisetty<sup>b,\*</sup> and Mikhael Bechelany<sup>a,\*</sup>

<sup>a</sup>*Institut Européen des Membranes, UMR 5635 ENSCM-UM-CNRS Université Montpellier, Place Eugene Bataillon, F-34095 Montpellier Cedex 5, France*

<sup>b</sup>*Department of Chemistry, Durban University of Technology, P.O. Box 1334, Durban 4000, South Africa*

†Corresponding authors. [mikhael.bechelany@umontpellier.fr](mailto:mikhael.bechelany@umontpellier.fr) (M. Bechelany), [bisettyk@dut.ac.za](mailto:bisettyk@dut.ac.za) (K. Bisetty)

### Abstract

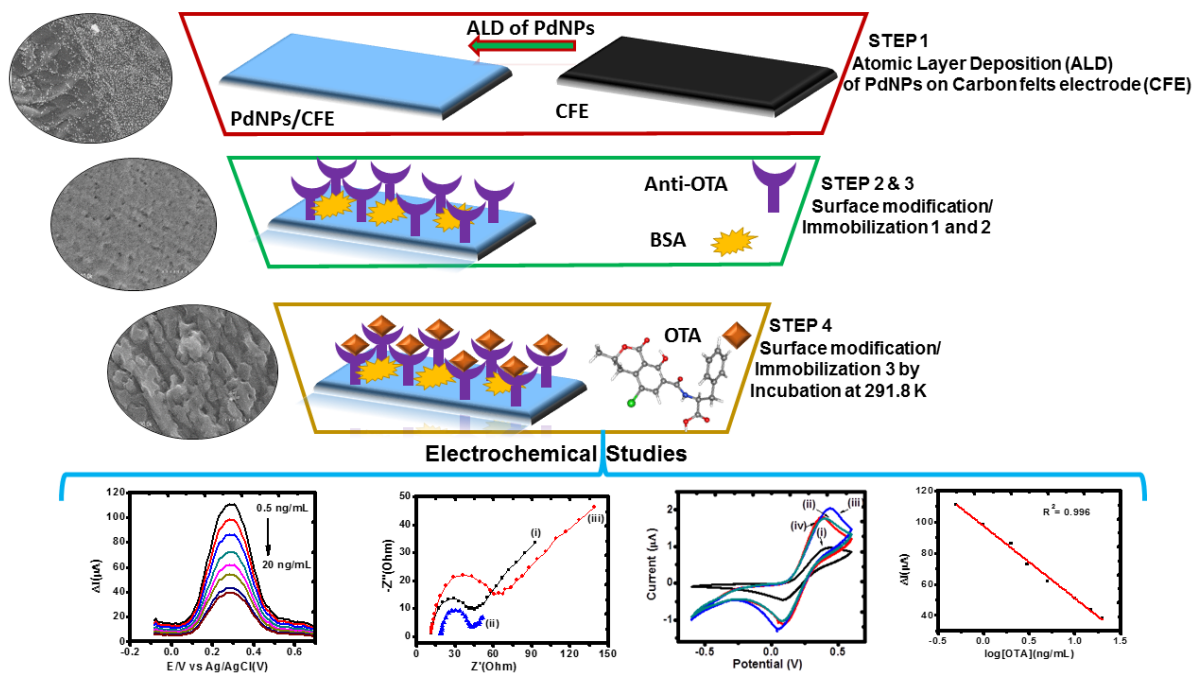
Ochratoxin A (OTA) is among the most important mycotoxins classified as potential risks to human health and food safety. In this work, a novel label-free electrochemical immunosensor has been proposed for the quantitative detection of OTA, based on a two-step strategy for the fabrication of the immunosensor. This involved coating of a carbon felt (CF) electrode with palladium nanoparticles (PdNPs) using atomic layer deposition (ALD), followed by the grafting of the anti-OTA antibodies onto the nanocomposite structure using a carbodiimide functional group via a cross linkage route. Cyclic voltammetry (CV) and electrochemical impedance spectroscopy (EIS) have been employed for the characterization of the immunosensor properties. The fabricated BSA/anti-OTA/PdNPs/CF immunosensor showed outstanding electrochemical performance towards the detection of OTA in spiked coffee samples. At the optimal working conditions, the linear detection range of the developed immunosensor was from 0.5-20 ng mL<sup>-1</sup> ( $R^2 = 0.996$ ) with a low detection limit of 0.096 ng mL<sup>-1</sup>, making it applicable to the screening of OTA in food products. In addition, the sensor was highly selective to OTA in the presence of interfering compounds and revealed stability

28 of up to three weeks, opening up prospects for the molecular sensing community and paving a  
29 new route for quality control in the food industry.

30

31 **Keywords:** Electrochemical immunosensor, Ochratoxin A, Carbon felts electrode, Palladium  
32 nanoparticles, Atomic Layer Deposition

33



34

35

## 36 1. Introduction

37

38 Ochratoxin A (OTA) is one of the secondary fungal metabolite that occurs naturally and is  
39 present in many food products and produced by a number of fungal species such as  
40 *Aspergillus ochraceus* and *Penicillium verrucosum* [1]. OTA is primarily found in food  
41 commodities such as cereals, coffee beans, and wine [2-4]. Different studies reported that  
42 OTA is among the most abundant and toxic mycotoxins due to their high hepatotoxic,  
43 nephrotoxic, teratogenic, and mutagenic effects to most mammalian species [5, 6]. They are  
44 suspected of being one of the main cause of immuno suppression and immuno toxicity [7],

45 therefore, policies have been implemented in order to limit their toxicity in food products. For  
46 example, the European Union (E.U.) has established maximum permitted limits for OTA  
47 depending on the food products: 5.0  $\mu\text{g kg}^{-1}$  for unprocessed cereals, 10.0  $\mu\text{g kg}^{-1}$  for dried  
48 fruits, 15.0  $\mu\text{g kg}^{-1}$  for spices, 2.0  $\text{mg mL}^{-1}$  for all types of wines and 10  $\text{ng mL}^{-1}$  for coffee  
49 beans [2, 8, 9]. Consequently, the development of suitable analytical techniques to efficiently  
50 monitor OTA concentrations in food products has become crucial.

51 Conventional analytical techniques for the determination of OTA involves thin layer  
52 chromatography (TLC) [10], gas chromatography (GC) [11], liquid chromatography mass  
53 spectrometry (LC/MS) [12], photoluminescence [13, 14], enzyme-linked immunosorbent  
54 assay (ELISA) [15] ultra high performance chromatography-tandem mass spectrometry  
55 (UHPLC-MS/MS) [16] and high performance liquid chromatography (HPLC) [17, 18].  
56 However, these techniques require extensive sample preparation, highly trained personnel and  
57 are time consuming and costly. Thus, alternative methods offering high sensitivity, cost-  
58 effectiveness, fast and portable detection such as fluorescence [19], chemiluminescence [20]  
59 or electrochemistry [21, 22] have been developed. Previous reports have shown that  
60 electrochemistry techniques are fast and sensitive (in the  $\text{ng mL}^{-1}$  range), but with limited  
61 selectivity. For this reason, a steady shift towards aptasensors or biosensor techniques has  
62 been implemented, opening new promising paths for analysts. [19, 23].

63 Previously, various nanomaterials have been used for the development of efficient  
64 electrochemical immunosensors for OTA detection in different food products [24, 25]. As  
65 reported by Taghdisi and co-workers [26], the use of nanoparticles in electrochemical sensing  
66 devices is an extremely promising prospect, since they are biocompatible and able to retain  
67 the biological activity upon absorption, to enable the direct electron transfer through the  
68 conducting tunnels and the enhancement of immobilization of antibodies [27, 28]. Bonel and

69 co-workers developed indirect and competitive electrochemical immunosensors for the  
70 detection of OTA in wheat, using screen-printed carbon electrode (SPCE) on which OTA  
71 were conjugated to bovine serum albumin (OTA-BSA) and gold nanoparticles (OTA-BSA-  
72 AuNPs). The immunosensor showed a linear detection range (LDR) of 0.3 to 8.5 ng mL<sup>-1</sup>,  
73 with a limit of detection (LOD) of 0.86 ng mL<sup>-1</sup> [25]. Another biosensor was reported by  
74 Rivas and co-workers where (SPCE) modified with polythionine (PTH) and iridium oxide  
75 nanoparticles (IrO<sub>2</sub> NPs) were used for the detection of OTA in wine samples. The label-free  
76 aptasensor showed the LDR of 0.004 and 40 ng mL<sup>-1</sup>, and found the lowest LOD reported so  
77 far for label-free impedimetric detection of OTA (14 pM) [24]. Karczmarczyk and co-workers  
78 developed a sensitive indirect competitive assay quartz crystal microbalance with dissipation  
79 monitoring (QCM-D) sensor for detection of OTA in red wine. They amplified the QCM-D  
80 signal by combining the secondary antibodies with gold nanoparticles (AuNPs), and found a  
81 LODs of 0.16 ng mL<sup>-1</sup> in the LDR of 0.2–40 ng mL<sup>-1</sup> [4]. Zhang and co-workers represents  
82 the amplified voltammetric immunoassay for OTA in red wine. They achieved this by  
83 enclosing platinum on gold cores (AuPtNP) and functionalized it with monoclonal antibodies.  
84 The system presented a LDR of 0.2 to 5×10<sup>3</sup> pg mL<sup>-1</sup> of OTA, with a lower LOD of 0.75 pg  
85 mL<sup>-1</sup> [29]. However, the above reported immunosensors for OTA detection were based on  
86 complex methods for synthesis of nanomaterials and were often fabricated using multiple  
87 routes. Thus, novel and easier routes enabling the fabrication of immunosensing devices are  
88 highly desired.

89 Atomic layer deposition (ALD) is a novel promising strategy for the direct growth of both  
90 thin films and nanoparticles with controllable dimensions at the nanometer scale [30, 31].  
91 This vapor phase technology is based on the sequential use of self-limiting chemical reactions,  
92 enabling the synthesis of high quality inorganic nanomaterials in challenging substrates, with

93 a precise control over their thickness. These benefits permitted this technique to become an  
94 essential tool for the deposition of nanomaterials for a myriad of applications, such as  
95 microelectronics [32], but also catalysis [33], membranes [34] and biosensing [35].

96 In the present work, we report a novel PdNPs/carbon nanocomposite based immunosensor for  
97 the efficient detection of OTA in coffee samples, using a two-step strategy for the fabrication  
98 of the immunosensor. Firstly, ALD was employed to coat CF substrates with highly dispersed  
99 palladium nanoparticles (PdNPs), and the anti-OTA were then grafted to the composite  
100 structure using a carbodiimide cross linkage route. Next, the composite structures were  
101 characterized in terms of physical and chemical properties, using scanning electron  
102 microscopy (SEM), transmission electron microscopy (TEM) and attenuated total reflectance  
103 (ATR). The immunosensor was then tested for the detection of OTA in spiked coffee samples  
104 using differential pulse voltammetry (DPV) and assessed on LODs, reproducibility and  
105 selectivity.

106

## 107 **2. Experimental section**

### 108 **2.1 Materials and methods**

109 The carbon felt (CF) AvCarb® MGL190 was purchased from Johnson Matthey Co.,  
110 Germany. Modified carbon felt electrode (CFE) were used as the working electrode, graphite  
111 rode as the counter electrode and Ag/AgCl as the reference electrode. The dimensions of the  
112 working electrode supports were 3.5 cm length, 0.7 cm width, and 0.3 cm thickness. *N*-(3-  
113 dimethylaminopropyl)-*N*'-ethycabordiimide (EDC)(CAS Number 1892-57-5, purity 97.0%),  
114 *N*-hydroxysuccinimide (NHS)(CAS Number 6066-82-6, purity 98.0%), potassium  
115 ferricyanide ( $K_3Fe(CN)_6$ ) (CAS Number 13746-66-2, purity 99.0%), potassium ferrocyanide  
116 ( $K_4Fe(CN)_6$ ) (CAS Number 14459-95-1, purity 98.5-102.0%), potassium hydrogen phosphate

117 (K<sub>2</sub>HPO<sub>4</sub>) (CAS Number 7758-11-4, purity 98.0%), potassium dihydrogen phosphate  
118 (KH<sub>2</sub>PO<sub>4</sub>) (CAS Number 7778-77-0, purity 99.0%), phosphate buffered saline tablet (PBS)  
119 (CAS Number 0000000000), palladium (II) hexafluoroacetylacetonate (Pd(hfac)<sub>2</sub> (CAS  
120 Number 64916-48-9, purity 99.0%), OTA standard solution (OTA), 1 mg mL<sup>-1</sup> in DMSO  
121 (CAS Number 303-47-9, purity 98.0%), formaldehyde solution (CH<sub>2</sub>O) (CAS Number 50-00-  
122 0, ACS reagent, 37 wt. % in H<sub>2</sub>O, contains 10-15% Methanol as stabilizer) and Bovine serum  
123 albumin solution (BSA) (CAS Number 9048-46-8, purity 98.0%) were purchased from  
124 Sigma-Aldrich, France. Monoclonal antibody anti-ochratoxin A (anti-OTA) (Catalog #:  
125 ICP9948, 250 μg mL<sup>-1</sup> in PBS 50% glycerol) was obtained from Immune Chem  
126 Pharmaceutical Incl (Canada). Nescafe (NES, Vevey, Switzerland) obtained from a local  
127 supermarket. Double distilled water was used for all experiments.

128

## 129 **2.2 Apparatus**

130 The modified CF electrodes were characterized by scanning electron microscopy  
131 (SEM, Hitachi S-4800). The contact angle (CA) measurements of PdNPs/CF and BSA/anti-  
132 OTA/PdNPs/CF electrodes were conducted on a homemade contact angle setup. During  
133 measurement, a drop of deionized water was deposited over the electrode surface and the  
134 angle of the liquid surface with contact surface was observed at the solid-liquid interface.  
135 attenuated total reflectance (ATR) spectra were collected using iS50 ATR Thermo scientific  
136 spectrophotometer. Electrochemical measurements such as cyclic voltammetry (CV),  
137 differential pulsed voltammetry (DPV) and electrochemical impedance spectroscopy (EIS)  
138 were performed at room temperature (~ 25.0 °C) using a SP-150 EC-LAB Electrochemistry  
139 chemical workstation (VSP Potentiostat from BioLogic Science Instruments, France).  
140 Transmission electron microscopy (TEM) was performed using a JEOL 2200FS (200 kV).

141

### 142 **2.3 Synthesis of palladium nanoparticles (PdNPs) by Atomic Layer Deposition (ALD)**

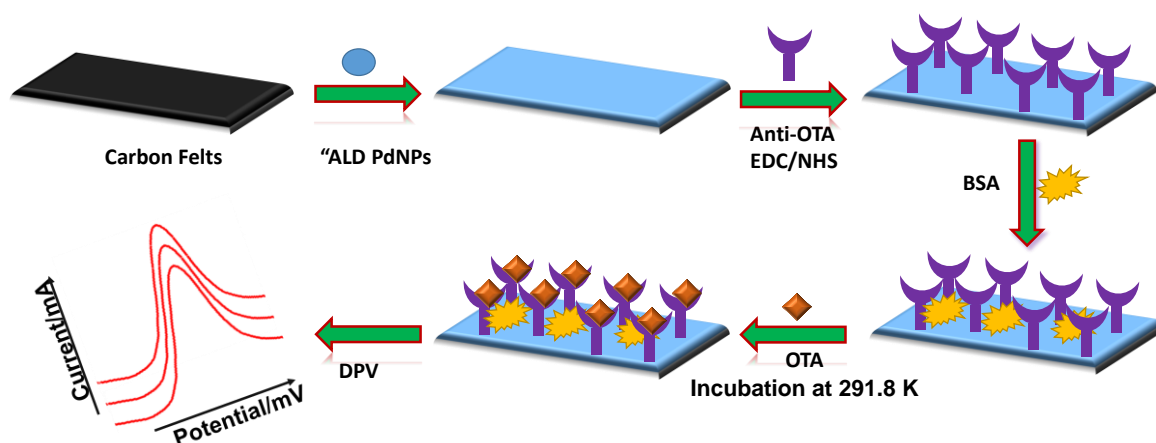
143 In this work, the highly dispersed PdNPs were synthesized by applying 200 ALD  
144 cycles in a low-pressure hot-wall (home-built) ALD reactor. ALD was achieved using  
145 sequential exposures of Pd(hfac)<sub>2</sub> and formalin separated by Argon purges. If not specified  
146 otherwise, the ALD cycle consisted of 5 s pulse of Pd(hfac)<sub>2</sub>, 15 s of gas exposure, 10 s of  
147 purge with Argon followed by 1 s pulse of formalin, 15 s of exposure and finally 60 s purge  
148 with Argon. Further details about both this deposition protocol and the associated ALD  
149 reactor can be found elsewhere [35, 36].

150

### 151 **2.4 Modification of PdNPs/CF with anti-OTA and BSA**

152 A fresh stock solution of anti-OTA (1.0 µg mL<sup>-1</sup>) was prepared in phosphate buffer  
153 saline solution (PBS) presenting a pH value of 7.4. The anti-OTA solution was mixed with  
154 0.4 M EDC and 0.1 M NHS in the ratio of 4:1:1 and kept at 4.0 °C for 30 min, to activate the  
155 carboxyl groups in fragment crystallizable (Fc) region of anti-OTA [37]. Thereafter, the anti-  
156 OTA was ready for the two steps immobilization process onto the surface of PdNPs/CF. In a  
157 first step, 10 µL of anti-OTA with EDC-NHS was spread over the PdNPs/CF electrode and  
158 incubated at 4.0 °C for 6.0 h, after which it was washed with PBS to remove the unbounded  
159 or excess anti-OTA from the electrode surface. Secondly, 10 µL of BSA (0.1 %) was spread  
160 over anti-OTA/PdNPs/CF immunoelectrode surface, to block any non-specific active sites on  
161 the electrode (Scheme 1). The fabricated BSA/anti-OTA/PdNPs/CF immunoelectrode was  
162 kept at 4.0 °C when not in use.





163

164 **Scheme 1:** Schematic representation of the preparation of BSA/anti-OTA/PdNPs/CF  
 165 immunoelectrode.

166

## 167 2.5 Preparation of coffee samples

168 The stock solution of the coffee sample ( $1.0 \text{ mg mL}^{-1}$ ) was prepared by ultrasonically  
 169 mixing 10 mL of PBS and 10 mg of coffee for 2 h. Thereafter 1.0 mL of the prepared  
 170 stock solution was spiked with different concentrations of OTA ranging from 0.5 to 20 ng  
 171  $\text{mL}^{-1}$ ) and kept at  $4.0 \text{ }^\circ\text{C}$  until further use.

172

## 173 2.6 Indirect detection of OTA

174 For the OTA measurements,  $10 \text{ } \mu\text{L}$  of OTA standards with different concentrations  
 175 ranging from 0.5 to  $20 \text{ ng mL}^{-1}$  in PBS was pipetted onto the surface of the BSA/anti-  
 176 OTA/PdNPs/CF immunoelectrodes and allowed to stand for 40 min at room temperature.  
 177 DPV was used for the quantification of OTA and the measurements were conducted using a

178 5.0 mM  $K_3Fe(CN)_6/K_4Fe(CN)_6$  (1:1) mixture in PBS (pH 7.0). The CVs were performed in  
179 5.0 mM  $K_3[Fe(CN)_6]$  supported by 1 M KCl in 0.1 M  $K_2HPO_4$ – $KH_2PO_4$  solution. The EIS  
180 measurement was performed in 1 M KCl containing equimolar  $[Fe(CN)_6]^{3-/4-}$  with AC  
181 frequency from 0.1 to  $10^5$  Hz.

182

### 183 3. Results and Discussion

184

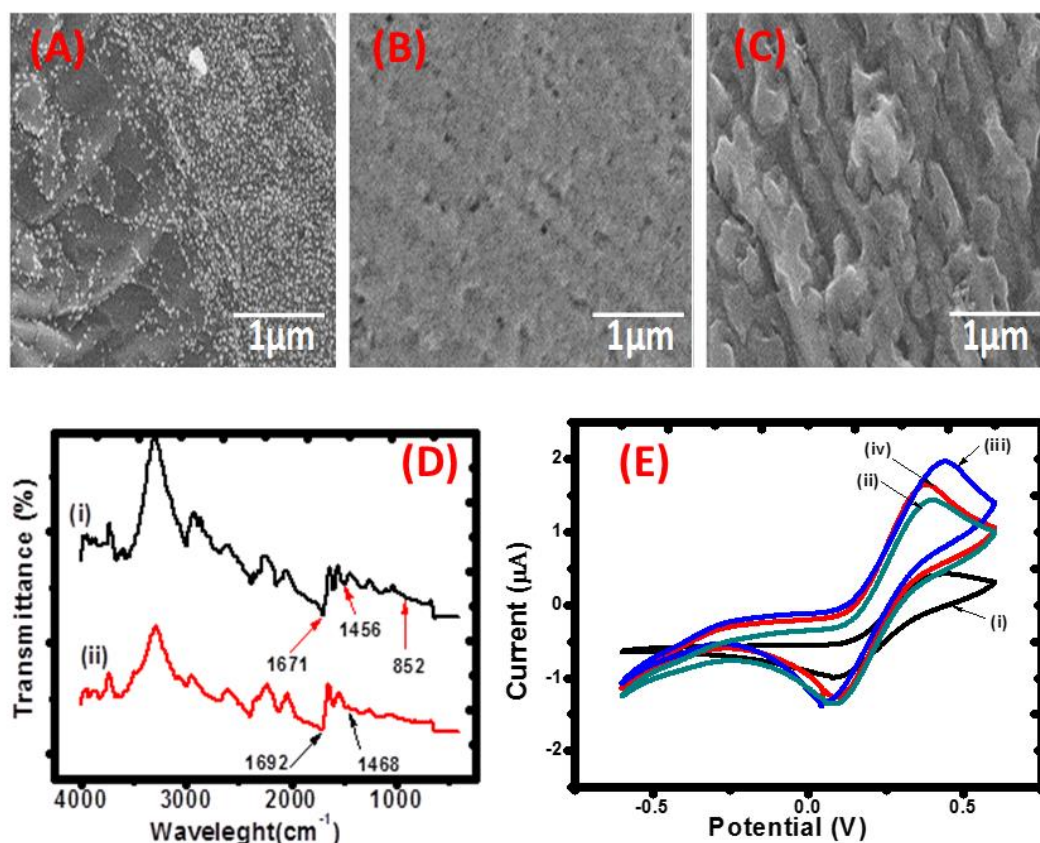
#### 185 3.1. Physical and chemical characterizations of the electrodes

186 Surface morphology of the fabricated electrodes were characterized by SEM and TEM.  
187 Fig 1A shows the morphology of PdNPs deposited onto CF by ALD over 200 cycles resulting  
188 in the formation of uniformly dispersed NPs. The TEM images (Fig.S1 A, B & C) further  
189 revealed an average diameter of  $6\pm 2$  nm for the PdNPs layer on the carbon substrate. It is  
190 clear from the SEM and the TEM images that the PdNPs were well-dispersed at the surface of  
191 the carbon substrate. These results were supported with X-Ray photoelectron microscopy to  
192 confirm the pure metallic form of Pd and inductively coupled plasma mass spectrometry  
193 (ICP-MS) to confirm the low metal loading limited at 0.85 wt.% ( $\pm 0.1$  %), corresponding to  
194  $< 0.1$  mgPd  $cm^{-2}$  [35].

195 After immobilization of BSA onto anti-OTA/PdNPs/CF electrode, a smooth surface  
196 morphology was obtained as shown in Fig. 1B. The BSA was used to block non-binding sites  
197 of the anti-OTA/PdNPs/CF immunoelectrode. Further immobilization of OTA by incubation  
198 onto BSA/anti-OTA/PdNPs/CF results in a rough surface as can be seen in Fig.1C, which is  
199 indicative of optimum adsorption of OTA on the electrode surface.

200 The functional groups present in the fabricated immunosensor were investigated by ATR,  
201 with Fig. 1D showing the anti-OTA/PdNPs/CF (curve i) and BSA/anti-OTA/PdNPs/CF

202 (curve ii). A characteristic peak at  $1671\text{ cm}^{-1}$  corresponding to  $\text{-NH}$  deformation in an amide-  
 203 II bond, suggesting the covalent immobilization of anti-OTA on the electrode surface (curve  
 204 i). The band seen around  $1456\text{ cm}^{-1}$  is due to the vibration of  $\text{-CH}_2$  aliphatic moiety of anti-  
 205 OTA [37]. The band found at  $852\text{ cm}^{-1}$  is due to free  $\text{-NH}_2$  groups on the electrode surface.  
 206 After BSA immobilization (curve ii; BSA/anti-OTA/PdNPs/CF), the band at  $852\text{ cm}^{-1}$   
 207 completely disappeared, this confirms the blocking of nonspecific sites available on anti-  
 208 OTA/PdNPs/CF immunoelectrode [38].



209  
 210 **Fig.1.** SEM images of PdNPs/CF electrode (A); BSA/anti-OTA/PdNPs/CF (B); and OTA/BSA/anti-  
 211 OTA/PdNPs/CF (C) immunoelectrode. (D) ATR spectra of anti-OTA/PdNPs/CF (i); and BSA/ant-  
 212 OTA/PdNPs/CF (ii) immunoelectrode; (E) CV comparison of CF electrode (i); PdNPs/CF (ii); anti-  
 213 OTA/PdNPs/CF (iii) and BSA/anti-OTA/PdNPs/CF (iv) immunoelectrodes in PBS containing 5.0 mM  
 214  $[\text{Fe}(\text{CN})_6]^{3-/4-}$  solution.

215

216 The hydrophobic/hydrophilic nature of the modified electrode was investigated by  
217 measuring the water contact angle (CA) of the PdNPs/CF and BSA/anti-OTA/PdNPs/CF  
218 electrodes. The CA represents the level of wetting property on the solid-liquid interaction. A  
219 CA value of 56.2° for PdNPs electrode (Fig. S2A) indicates a reasonable hydrophilicity  
220 however, after immobilization of anti-OTA onto the PdNPs/CF electrode (Fig S2B) the CA  
221 value decreased to 14.3°, indicating that anti-OTA further enhanced the wettability properties  
222 of the electrode.

223

## 224 **3.2. Electrochemical studies**

### 225 **3.2.1. Electrodes characterization through cyclic voltammetry (CV)**

226 CV is one of the most convenient technique that is used to monitor the behavior of the  
227 modified electrode. Fig. 1 (E) shows the CV response obtained using 5.0 mM  $[\text{Fe}(\text{CN})_6]^{3-/4-}$  in  
228 PBS for (i) CF (ii), PdNPs/CF (iii) anti-OTA/PdNPs/CF and (iv) BSA/anti-OTA/PdNPs/CF  
229 immunoelectrodes. A pair of well-defined redox peak was observed for the CF (curve i), This  
230 quasi-reversible redox peak was attributed to the transformation between  $\text{Fe}(\text{CN})_6^{4-}$  and  
231  $\text{Fe}(\text{CN})_6^{3-}$ . The low anodic peak current ( $I_{pa}$ ) of 0.99  $\mu\text{A}$  and 1.03  $\mu\text{A}$  for the bare CF  
232 electrode and anti-OTA/CFE immunoelectrode demonstrates a poor electrochemical response  
233 of the CF electrode and hindrance of electron transfer caused by the insulation and steric  
234 hindrance produced by anti-OTA. On the other hand, the  $I_{pa}$  increased to 1.77  $\mu\text{A}$  for the  
235 PdNPs/CF coated surface (curve ii). These results demonstrate that deposition of PdNPs onto  
236 the CF substrate accelerates the rate of electron transfer between analyte and working  
237 electrode, due to high surface area and improvement in catalytic activity of the electrode.

238 However, when anti-OTA were immobilized onto the PdNPs/CF electrode the  $I_{pa}$  increased to  
239 2.05  $\mu\text{A}$  (curve iii), indicating further enhanced sensitivity. This phenomenon is probably due  
240 to the fragmented crystalline (Fc) region of the anti-OTA and the amine groups that forms a  
241 penetrating path between anti-OTA and electrode [37]. The free site amino group of anti-OTA  
242 available onto immunoelectrode surface electrostatically interacts with redox species of  
243 electrolyte and facilitates the fast electron diffusion at the electrode. However, for the  
244 BSA/anti-OTA/PdNPs/CF electrode the  $I_{pa}$  decreased to 1.83  $\mu\text{A}$  (curve iv), this is in  
245 agreement with the previous report stating that BSA inhibiting the diffusion of redox species  
246 towards the electrode [39]. Our results confirmed the successful fabrication of the BSA/anti-  
247 OTA/PdNPs/CF immunoelectrode.

248

### 249 3.2.2. Effects of scan rate

250 Cyclic voltammetry was used to study the interface kinetics of BSA/anti-  
251 OTA/PdNPs/CF immunoelectrode by varying scan rate from 10-100 mV/s as shown in Fig.  
252 S3A. The peak currents increase linearly with the increase of scan rates while there was a  
253 minor shift of peak potential towards more a positive potential and more faradic current is  
254 flowing on the electrode. This indicates that the electroactive species are confined at the  
255 electrode surface and the reaction of OTA is following an adsorption-controlled process [40].

256

### 257 3.2.3. Electrochemical impedance spectroscopy

258 Electrochemical impedance spectroscopy results are presented using a Nyquist plot of CF  
259 with different modification processes using  $[\text{Fe}(\text{CN})_6]^{3-/4-}$  as the electrolyte. EIS spectrum  
260 comprises of a semicircle and the linear part as illustrated in Figures 2A-B. The semicircle  
261 diameter represents the electron-transfer resistance ( $R_{ct}$ ) and reveals the restricted diffusion of

262 the electrolyte through the multilayer system, directly related to the film permeability. A very  
263 small semicircle diameter is observed on anti-OTA/CF electrode Fig. S6A demonstrating a  
264 low charge transfer resistance for the electrochemical process. At low frequency, the linear  
265 part is associated with the mass transfer process. After the deposition of PdNPs on the CF, the  
266 capacitance increases. Fig. 2B (curve i) shows the modification with PdNPs increases the  
267 electrochemical active surface area. The amplification of electrochemical signal and the  
268 enhancement of the electron transfer rate of the sensor are due to the excellent electro-  
269 catalytic activity of PdNPs [41]. After immobilization of anti-OTA (curve ii) onto PdNPs/CF  
270 electrode, a remarkable decrease of the charge transfers resistance ( $R_{ct}$ ) is observed. This  
271 phenomenon is attributed to the presence of positively charged amino residues on the  
272 antibody structure, which facilitates the electrochemical reaction [42]. The increased in  
273 electron transfer observed can also be attributed to the neutralization of surface negative  
274 charge upon reaction with EDC/Sulfo-NHS [43].

275 However, after immobilization of BSA (curve (iii)), both  $R_{ct}$  and the capacitance increased,  
276 due to the longer path for the electrons to move from the solution to the surface of the  
277 electrode. The EIS data in Fig. 2 (A and B) were further analyzed by fitting them to the  
278 simulation data using the equivalent circuit model shown in Fig. 2 (B) inset. The fitting  
279 parameters include the ohmic resistance of the electrolyte solution ( $R_s$ ), C is the capacitance  
280 that arises due to coverage of the electrode surface with BSA,  $R_{ct}$  is a charge transfer  
281 resistance that is caused by the resistance of electrons between electrode and  $Fe(CN)_6^{3-/4-}$   
282 redox probe, R is electrolyte resistance in the pore and Q is the CPE arising due to CF surface  
283 and Warburg impedance (W). Yang and co-workers reported the similar equivalent circuit on  
284 their work, their equivalent fitting has, the interface ohmic resistance ( $R_d$ ), double layer  
285 capacitances ( $CPE_{dl}$ ) and pore adsorption capacitance ( $CPE_{ad}$ ) [44]. Siddiqui also reported the

286 similar equivalent circuit that has the uncompensated resistance  $R_s$ , capacitance  $C$ , charge  
287 transfer resistance  $R_{ct}$ ,  $R$  is electrolyte resistance in the pore and  $Q$  [45]. BSA layer makes the  
288 electrode surface more homogenous and generates the capacitance of  $0.4 \times 10^{-8}$  F. Therefore,  
289 BSA behaves as an insulator. Moreover, the ohmic resistance ( $R_s$ ) of BSA/anti-  
290 OTA/PdNPs/CF is estimated to be  $\sim 8.06$  ohms, much lower than that of CF materials ( $\sim 19.22$   
291 ohms) and PdNPs ( $\sim 10.7$  ohms).

292

### 293 **3.2.4. Effect of pH**

294 The pH is a key parameter when fabricating an immunosensor electrode, due to the strong  
295 influence of the electrolyte on the electrochemical performance. This parameter was  
296 investigated by monitoring the current response of immunoelectrodes in electrolytes in the  
297 range of pH 6.0 - 8.0. In Fig. 2C the peak currents response increase from pH 6.0 to 7.0, then  
298 gradually decreases beyond pH 7.0. This indicates that biomolecules on the electrode surface  
299 can only provide optimum performance when they are on their original form at neutral pH as  
300 the basic or acidic medium denatures them due to the interaction of  $H^+$  or  $OH^-$  ion with amino  
301 acid sequence of antibodies (anti-OTA) [39, 46]. The maximum value of the peak current was  
302 observed at pH 7.0 and therefore it was selected as the optimum pH for the subsequent  
303 experiments.

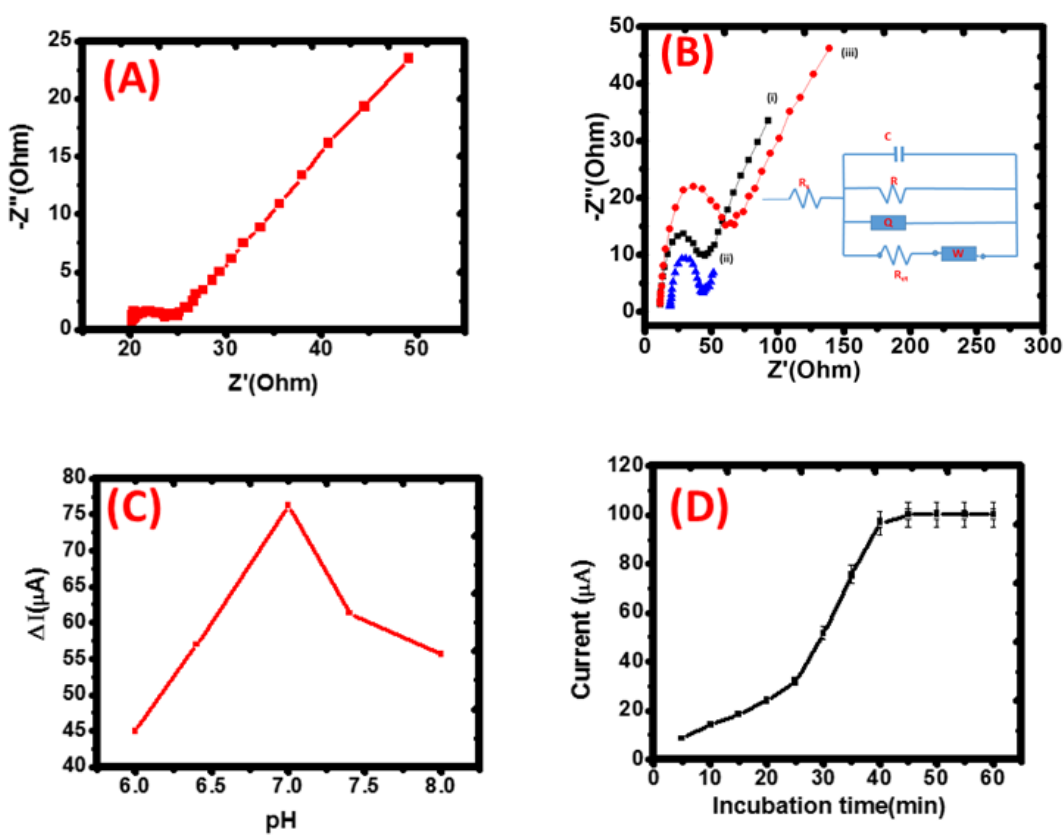
304

### 305 **3.2.5. Effect of incubation time**

306 The immunochemical reaction is the process whereby the antigen and antibody interacts  
307 with each other to form the immunocomplex. Its formation depends on the interaction time  
308 (incubation time) of the antibody and antigen. Therefore, in order to get the optimum value of

309 the incubation time, measurements of  $1.0 \text{ ng mL}^{-1}$  OTA on BSA/anti-OTA/PdNPs/CF  
 310 immunoelectrode were recorded every 5 min for a duration of 60 min as shown in Fig. 2D. It  
 311 was observed that the peak current rises with an increase in interaction time of the  
 312 immunocomplex up to 40 min. Beyond 40 min, it remains constants due to the saturation of  
 313 antibodies. Subsequently, duration of 40 min was selected as the optimum interaction time for  
 314 the immunochemical interaction.

315



316

317

318 **Fig. 2** (A) Nyquist plots of bare CF electrode; (B) PdNPs/CF (i); anti-OTA/PdNPs/CF (ii)  
 319 and BSA/anti-OTA/PdNPs/CF (iii) modified electrode in PBS, pH 7.0., containing 5.0  
 320 mM  $[\text{Fe}(\text{CN})_6]^{4-/3-}$  solution: the inset shows the used equivalent circuit. (C) DPV response  
 321 of BSA/anti-OTA/PdNPs/CF immunoelectrode of electrolyte pH and (D) incubation time.

322

323

324

325

326



327

### 328 3.2.6. Effects of anti-OTA concentration

329 The sensitivity of the immunosensor depends on the immunochemical reaction between  
330 the antigen and antibody (anti-OTA). The concentration of the antibody on the electrode  
331 surface is one of the most vital factors for the performance of the immunosensor. The effects  
332 of anti-OTA concentration on the immunoelectrode were investigated by immobilizing four  
333 different concentrations (0.5, 1, 5 and 10  $\mu\text{g mL}^{-1}$ ) of anti-OTA onto the PdNPs/CF electrode.  
334 The DPV responses of OTA were measured from 0.5  $\text{ng mL}^{-1}$  to 2.5  $\text{ng mL}^{-1}$ , in order to  
335 check the sensitivity of the fabricated immunoelectrodes. The change in current (denoted as  
336  $\Delta C$ ), measured before and after immunoreaction, was calculated according to equation (1):

$$337 \quad \Delta C = C_{\text{anti-OTA}^{\prime}\text{OTA}} - C_{\text{anti-OTA}} \quad (1)$$

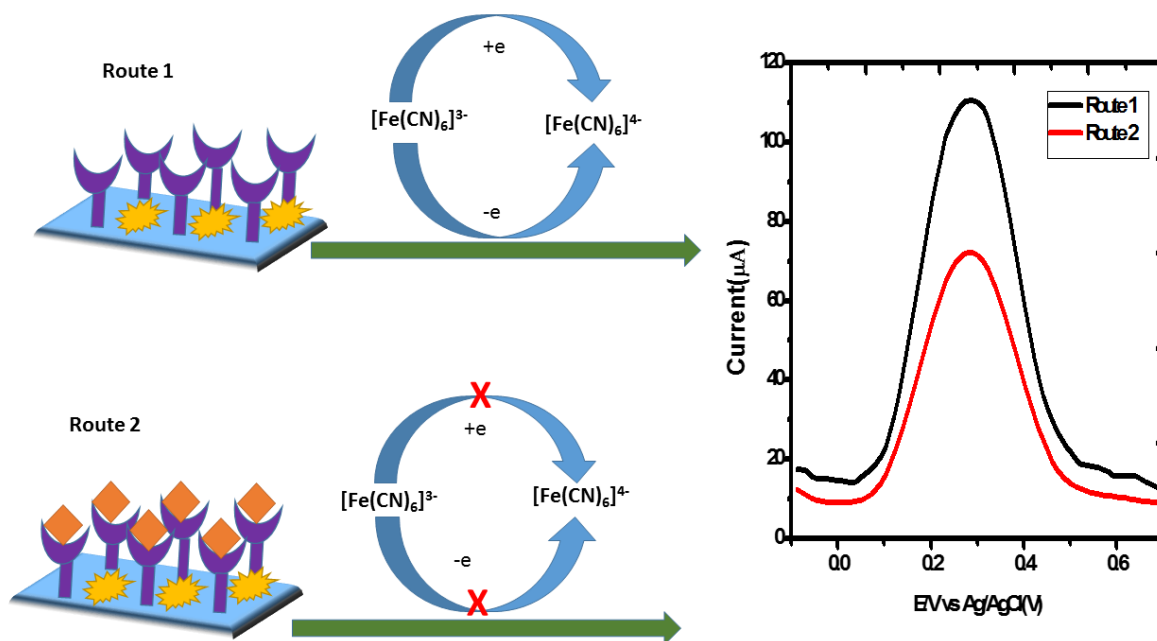
338 where  $C_{\text{anti-OTA}^{\prime}\text{OTA}}$  is the value of the current after OTA coupling to the anti-OTA and  $C_{\text{anti-OTA}}$   
339 represents the value of the current of the native immunosensor. The immunosensor with  
340 1.0  $\mu\text{g mL}^{-1}$  anti-OTA showed significant decrease in the current resulting in the LOD (0.25  
341  $\text{ng mL}^{-1}$ ) and regression coefficient ( $R^2$ ) of 0.9980 as shown in Fig. S3B and Table S1.  
342 However, the immunosensor with 5.0  $\mu\text{g mL}^{-1}$  and 10  $\mu\text{g mL}^{-1}$  anti-OTA concentrations  
343 showed a lower current with LODs and regression coefficients ( $R^2$ ) of (0.39  $\text{ng mL}^{-1}$ , 0.9850  
344 and 0.44  $\text{ng mL}^{-1}$  0.9234 respectively. This is attributed to dense electrode surface with an  
345 inadequate binding between the antigen and antibody to cause a current change. Therefore,  
346 the thicker bioactive layer is the cause of a low performance of the immunosensor. Hence, 1.0  
347  $\mu\text{g mL}^{-1}$  anti-OTA was chosen as the optimal concentration for the further characterization of  
348 the immunosensor.

349

350

351 **3.2.7. Sensing mechanisms of the immunosensor**

352 In this work, the immunosensor was fabricated by covalently attaching antibody (Anti-  
353 OTA) to the PdNPs coated CF electrode surface. The PdNPs are employed as the carriers of  
354 the electrochemical capture probe to increase the change of peak currents. The ferricyanide  
355 solution is used as a redox mediator to generate the electron flow between bulk solution and  
356 working electrode as shown in Scheme 2. In the absence of OTA, the Anti-OTA offer a  
357 significantly strong Faradaic current. However, in the presence of OTA the faradic current  
358 decreases because, the formation of anti-OTA/OTA complex hinders the electron-transfer of  
359  $\text{Fe}(\text{CN})_6^{3-}/\text{Fe}(\text{CN})_6^{4-}$  [47, 48].



360  
361 **Scheme 2:** The mechanism of the electrochemical immunosensor for the indirect detection of  
362 OTA.

363

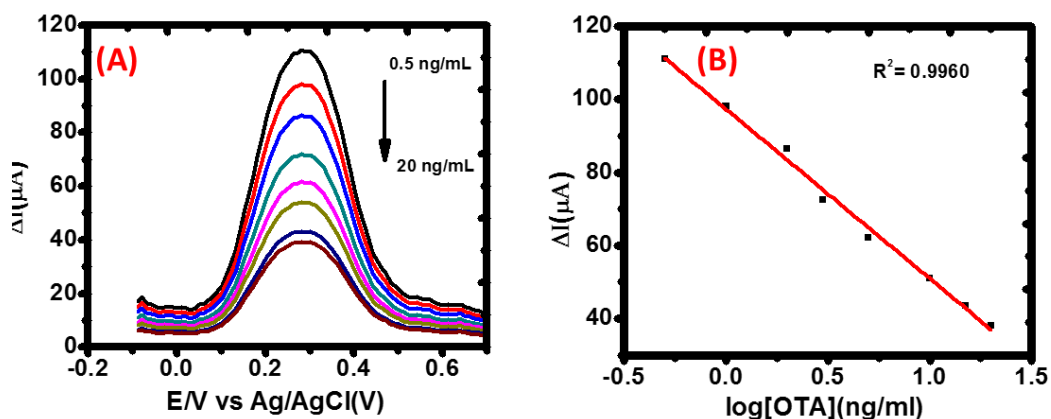
364

365

### 366 3.2.8. Indirect quantification of OTA

367 The DPV response of BSA/anti-OTA/PdNPs/CF immunoelectrode recorded as a function of  
368 OTA concentration ranging from 0.5 to 20 ng mL<sup>-1</sup> are depicted in Figure 3. The peak current  
369 ( $\Delta I$ ) decreased with an increase in OTA concentration, showing the formation of  
370 immunocomplex (antigen-antibody) at the electrode surface. This was established through the  
371 interaction of antigen with the antibody (anti-OTA) absorbed onto the BSA/anti-  
372 OTA/PdNPs/CF immunoelectrode which acts as an electron transporting layer [49, 50]. The  
373 resulting DPV measurements were then used to plot the calibration curve for OTA. The  
374 fabricated immunosensor BSA/anti-OTA/PdNPs/CF responds linearly to the logarithm  
375 concentration of OTA ranging from 0.5 to 20 ng mL<sup>-1</sup> with LOD of 0.096 ng mL<sup>-1</sup> (3 $\times$ se)/m  
376 and a regression coefficient ( $R^2$ ) of 0.9960 [Fig. 3B].

377 The biosensing parameters of the fabricated immunosensor were then compared to the  
378 previously reported immunosensors for the detection of OTA (data given in Table S2). The  
379 fabricated BSA/anti-OTA/PdNPs/CF immunoelectrode have the ability to detect a very low  
380 concentration (96 pg mL<sup>-1</sup>) of OTA as compared to other immunosensors [5, 8]. These results  
381 show that PdNPs/CF materials provide high surface affinity to bind antibodies.



382

383 **Fig. 3.** (A) Electrochemical response studies of the BSA/anti-OTA/PdNPs/CF  
 384 immunoelectrode as a function of OTA using DPV (Conditions: Scan rate:  $30 \text{ mV s}^{-1}$ ,  
 385 Deposition time: 80 s, Pulse amplitude: 0.08 V and Pulse time: 0.03 s and (B) calibration  
 386 curve between the magnitude of current and OTA concentration.

387

### 388 3.2.9. Recovery studies for the real samples

389 In order to investigate the ability of the fabricated BSA/anti-OTA/PdNPs/CF  
 390 immunoelectrode, DPV responses were recorded in the presence of different concentrations of  
 391 the spiked coffee samples. Table 1 shows the outcomes of the recovery studies for spiked  
 392 sample in terms of electrochemical current. The DPV response was observed using five  
 393 concentrations ( $0.5, 1, 5, 10, 20 \text{ ng mL}^{-1}$ ), and the recovery was found in the range of 93.2-  
 394 98.9 % with proportional error ranging from 1.0 to 6.8 %. These measured values of RSD and  
 395 recovery were quite good and suggest that fabricated immunoelectrode is appropriate to be  
 396 applied to OTA detection.

397

398 **Table 1:** Determination of OTA concentration in spiked samples using BSA/anti-OTA/PdNPs/CF  
 399 immunoelectrode

Spiked concentration (ng/mL)	DPV response for		Recovery (%)	Proportional error (%)
	Spiked sample ( $\mu$ A)	OTA ( $\mu$ A)		
0.5	98.45	100.56	97.9	2.1
1	95.70	96.70	98.9	1.0
5	58.78	63.10	93.2	6.9
10	42.40	43.60	97.3	2.8
20	36.89	38.15	96.7	3.3

400

### 401 **3.2.10. Selectivity and shelf-life of immunoelectrode**

402 Selectivity and shelf-life are also very important parameters of immunoelectrodes. The  
 403 selectivity of the immunoelectrode was investigated by monitoring the DPV response of  
 404 BSA/anti-OTA/PdNPs/CF in the presence of the interferences. Different interferences such as  
 405 BSA, Aflatoxin B1 and L-Tryptophan ( $10 \text{ ng mL}^{-1}$ ) were mixed with OTA ( $1 \text{ ng mL}^{-1}$ ), and the  
 406 DVP response was assessed (Fig. S4B). There was no significant change in the DPV response  
 407 after the interaction of the immunoelectrode with interfering compounds. This indicates that  
 408 the fabricated immunoelectrode is only selective to OTA detection. The DPV technique was  
 409 used to investigate the shelf-life of immunoelectrode on a regular interval of seven days up to  
 410 three weeks using the optimized parameters. The fabricated immunoelectrode shown in Fig.  
 411 S4A shows that is stable up to at least three weeks, with a slight change in current value (99.6  
 412 %) was observed. This suggests that BSA/anti-OTA/PdNPs/CF immunoelectrode is highly  
 413 stable.

414

### 415 **3.3. Reproducibility and repeatability of immunoelectrode**

416 The reproducibility of the BSA/anti-OTA/PdNPs/CF immunoelectrode was studied using  
417 the interassay methods where DPV response was studied for six individual immunoelectrodes  
418 prepared independently as shown in Fig.S5A. The value of relative standard deviation (RSD)  
419 was found to be 5.6 %. Additionally, the repeatability of the immunoelectrode was  
420 investigated using one immunoelectrode for six successive measurements, and the results  
421 showed a good standard deviation of 1.4% as shown in Fig. S5B. The repeatability results  
422 show that the fabricated immunosensor can be reusable. In fact, the repeatability of the  
423 fabricated immunosensor shows that the standard deviation is below 2%, after six successive  
424 measurements conducted on one immunosensor. Further study would however be needed for  
425 a more precise understanding the reusability of the fabricated immunosensor.

426

### 427 **Conclusion**

428 In this study, we reported the fabrication and the characterization of a novel and highly  
429 efficient electrochemical immunosensor for the selective detection of OTA. Atomic layer  
430 deposition has been successfully used as an efficient route to produce highly dispersed PdNPs  
431 onto the surface of carbon felt (CF) electrodes, and the BSA and the anti-OTA antibodies  
432 were then grafted onto the composite structure via a carbodiimide cross linkage route.  
433 Subsequently, the developed immunosensor was used to detect the OTA in coffee samples.  
434 The fabricated BSA/anti-OTA/PdNPs/CF immunosensor showed outstanding electrochemical  
435 performances such as a wide detection range of 0.5-20 ng mL<sup>-1</sup> and a LOD of 0.096 ng mL<sup>-1</sup>  
436 towards the detection of OTA. This study also revealed that the PdNPs accelerate the electron

437 transfer rate on the large surface area electrodes. Additionally, the immobilization of anti-  
438 OTA on the surface of the electrodes offer specific intrinsic immuno-recognition, with an  
439 improved binding efficiency, wettability property and enhanced selectivity of the sensor.  
440 Finally, this study also revealed that the fabricated immunosensor were selective to OTA in  
441 the presence of interfering compounds and that the sensors were stable for up to three weeks.  
442 The results presented in this work open prospects for new sensing routes for molecules of  
443 interest in food products.

444

#### 445 **Acknowledgements**

446 This work was financially supported by the French Embassy in South Africa through PhD  
447 scholarship, by the Council for Scientific and Industrial Research (CSIR, South Africa) and  
448 by the French National Agency (ANR, program MeNiNA - ANR-17-CE09-0049). The  
449 authors thank Bruno Navarra for technical support.

450

451

452

453

454

455

456

457

458

459

460

461

462

463

464

465

466

467

469 **References**

- 470 [1] J.C. Vidal, L. Bonel, A. Ezquerro, P. Duato, J.R. Castillo, An electrochemical  
471 immunosensor for ochratoxin A determination in wines based on a monoclonal antibody and  
472 paramagnetic microbeads, *Analytical and bioanalytical chemistry*, 403 (2012) 1585-1593.
- 473 [2] K.F. Nielsen, A.F. Ngemela, L.B. Jensen, L.S. De Medeiros, P.H. Rasmussen, UHPLC-  
474 MS/MS determination of ochratoxin A and fumonisins in coffee using QuEChERS extraction  
475 combined with mixed-mode SPE purification, *Journal of agricultural and food chemistry*, 63  
476 (2015) 1029-1034.
- 477 [3] X. Liu, Z. Tang, Z. Duan, Z. He, M. Shu, X. Wang, S.J. Gee, B.D. Hammock, Y. Xu,  
478 Nanobody-based enzyme immunoassay for ochratoxin A in cereal with high resistance to  
479 matrix interference, *Talanta*, 164 (2017) 154-158.
- 480 [4] A. Karczmarczyk, K. Haupt, K.-H. Feller, Development of a QCM-D biosensor for  
481 Ochratoxin A detection in red wine, *Talanta*, 166 (2017) 193-197.
- 482 [5] P.K. Gupta, N. Pachauri, Z.H. Khan, P.R. Solanki, One pot synthesized zirconia  
483 nanoparticles embedded in amino functionalized amorphous carbon for electrochemical  
484 immunosensor, *Journal of Electroanalytical Chemistry*, 807 (2017) 59-69.
- 485 [6] A. Karczmarczyk, A.J. Baeumner, K.-H. Feller, Rapid and sensitive inhibition-based assay  
486 for the electrochemical detection of Ochratoxin A and Aflatoxin M1 in red wine and milk,  
487 *Electrochimica Acta*, 243 (2017) 82-89.
- 488 [7] A. Kaushik, P.R. Solanki, A.A. Ansari, S. Ahmad, B.D. Malhotra, Chitosan-iron oxide  
489 nanobiocomposite based immunosensor for ochratoxin-A, *Electrochemistry Communications*,  
490 10 (2008) 1364-1368.
- 491 [8] F. Malvano, D. Albanese, R. Pilloton, M. Di Matteo, A highly sensitive impedimetric  
492 label free immunosensor for Ochratoxin measurement in cocoa beans, *Food chemistry*, 212  
493 (2016) 688-694.
- 494 [9] E. Commission, Commission Regulation (EC) No 1881/2006 of 19 December 2006  
495 setting maximum levels for certain contaminants in foodstuffs, *Off J Eur Union*, 364 (2006).
- 496 [10] A. Pittet, D. Royer, Rapid, low cost thin-layer chromatographic screening method for the  
497 detection of ochratoxin A in green coffee at a control level of 10 µg/kg, *Journal of*  
498 *Agricultural and Food Chemistry*, 50 (2002) 243-247.
- 499 [11] Y. Rodríguez-Carrasco, G. Font, J. Mañes, H. Berrada, Determination of mycotoxins in  
500 bee pollen by gas chromatography-tandem mass spectrometry, *Journal of agricultural and*  
501 *food chemistry*, 61 (2013) 1999-2005.
- 502 [12] S. Ahn, S. Lee, J. Lee, B. Kim, Accurate determination of ochratoxin A in Korean  
503 fermented soybean paste by isotope dilution-liquid chromatography tandem mass  
504 spectrometry, *Food chemistry*, 190 (2016) 368-373.
- 505 [13] R. Viter, M. Savchuk, I. Iatsunskyi, Z. Pietralik, N. Starodub, N. Shpyrka, A.  
506 Ramanaviciene, A. Ramanavicius, Analytical, thermodynamical and kinetic characteristics of  
507 photoluminescence immunosensor for the determination of Ochratoxin A, *Biosensors and*  
508 *Bioelectronics*, 99 (2018) 237-243.
- 509 [14] V. Myndrul, R. Viter, M. Savchuk, N. Shpyrka, D. Erts, D. Jevdokimovs, V. Silamiķelis,  
510 V. Smyntyna, A. Ramanavicius, I. Iatsunskyi, Porous silicon based photoluminescence  
511 immunosensor for rapid and highly-sensitive detection of Ochratoxin A, *Biosensors and*  
512 *Bioelectronics*, 102 (2018) 661-667.
- 513 [15] Z. Sun, X. Wang, Z. Tang, Q. Chen, X. Liu, Development of a biotin-streptavidin-  
514 amplified nanobody-based ELISA for ochratoxin A in cereal, *Ecotoxicology and*  
515 *environmental safety*, 171 (2019) 382-388.



516 [16] A.L. Manizan, M. Oplatowska-Stachowiak, I. Piro-Metayer, K. Campbell, R. Koffi-  
517 Nevry, C. Elliott, D. Akaki, D. Montet, C. Brabet, Multi-mycotoxin determination in rice,  
518 maize and peanut products most consumed in côte d'ivoire by uhplc-ms/ms, *Food control*, 87  
519 (2018) 22-30.

520 [17] M.A. Andrade, F.M. Lanças, Determination of Ochratoxin A in wine by packed in-tube  
521 solid phase microextraction followed by high performance liquid chromatography coupled to  
522 tandem mass spectrometry, *Journal of Chromatography A*, 1493 (2017) 41-48.

523 [18] M.L. Savastano, I. Losito, S. Pati, Rapid and automatable determination of ochratoxin A  
524 in wine based on microextraction by packed sorbent followed by HPLC-FLD, *Food Control*,  
525 68 (2016) 391-398.

526 [19] J. Zhang, Y.-K. Xia, M. Chen, D.-Z. Wu, S.-X. Cai, M.-M. Liu, W.-H. He, J.-H. Chen, A  
527 fluorescent aptasensor based on DNA-scaffolded silver nanoclusters coupling with Zn (II)-ion  
528 signal-enhancement for simultaneous detection of OTA and AFB1, *Sensors and Actuators B:*  
529 *Chemical*, 235 (2016) 79-85.

530 [20] E.-J. Jo, H. Mun, S.-J. Kim, W.-B. Shim, M.-G. Kim, Detection of ochratoxin A (OTA)  
531 in coffee using chemiluminescence resonance energy transfer (CRET) aptasensor, *Food*  
532 *chemistry*, 194 (2016) 1102-1107.

533 [21] M. Heurich, M.K.A. Kadir, I.E. Tohill, An electrochemical sensor based on  
534 carboxymethylated dextran modified gold surface for ochratoxin A analysis, *Sensors and*  
535 *Actuators B: Chemical*, 156 (2011) 162-168.

536 [22] H. Zejli, K.Y. Goud, J.L. Marty, Label free aptasensor for ochratoxin A detection using  
537 polythiophene-3-carboxylic acid, *Talanta*, 185 (2018) 513-519.

538 [23] N. Liu, D. Nie, Y. Tan, Z. Zhao, Y. Liao, H. Wang, C. Sun, A. Wu, An ultrasensitive  
539 amperometric immunosensor for zearalenones based on oriented antibody immobilization on  
540 a glassy carbon electrode modified with MWCNTs and AuPt nanoparticles, *Microchimica*  
541 *Acta*, 184 (2017) 147-153.

542 [24] L. Rivas, C.C. Mayorga-Martinez, D. Quesada-González, A. Zamora-Gálvez, A. de la  
543 Escosura-Muñiz, A. Merkoçi, Label-free impedimetric aptasensor for ochratoxin-A detection  
544 using iridium oxide nanoparticles, *Analytical chemistry*, 87 (2015) 5167-5172.

545 [25] L. Bonel, J.C. Vidal, P. Duato, J.R. Castillo, Ochratoxin A nanostructured  
546 electrochemical immunosensors based on polyclonal antibodies and gold nanoparticles  
547 coupled to the antigen, *Analytical Methods*, 2 (2010) 335-341.

548 [26] S.M. Taghdisi, N.M. Danesh, H.R. Beheshti, M. Ramezani, K. Abnous, A novel  
549 fluorescent aptasensor based on gold and silica nanoparticles for the ultrasensitive detection  
550 of ochratoxin A, *Nanoscale*, 8 (2016) 3439-3446.

551 [27] V. Solano-Umaña, J. Vega-Baudrit, Gold and silver nanotechnology on medicine,  
552 *Journal of Chemistry and Biochemistry*, 3 (2015) 21-33.

553 [28] A. Tiwari, M. Ramalingam, H. Kobayashi, A.P. Turner, *Biomedical materials and*  
554 *diagnostic devices*, John Wiley & Sons 2012.

555 [29] C. Zhang, J. Tang, L. Huang, Y. Li, D. Tang, In-situ amplified voltammetric  
556 immunoassay for ochratoxin A by coupling a platinum nanocatalyst based enhancement to a  
557 redox cycling process promoted by an enzyme mimic *Microchimica Acta*, 184 (2017) 2445-  
558 2453.

559 [30] M. Weber, M. Verheijen, A. Bol, W. Kessels, Sub-nanometer dimensions control of  
560 core/shell nanoparticles prepared by atomic layer deposition, *Nanotechnology*, 26 (2015)  
561 094002.

562 [31] S.M. George, Atomic layer deposition: an overview, *Chemical reviews*, 110 (2009) 111-  
563 131.

564 [32] I.J. Raaijmakers, Current and future applications of ALD in micro-electronics, ECS  
565 Transactions, 41 (2011) 3-17.

566 [33] A.J. Mackus, M.J. Weber, N.F. Thissen, D. Garcia-Alonso, R.H. Vervuurt, S. Assali,  
567 A.A. Bol, M.A. Verheijen, W.M. Kessels, Atomic layer deposition of Pd and Pt nanoparticles  
568 for catalysis: on the mechanisms of nanoparticle formation, Nanotechnology, 27 (2015)  
569 034001.

570 [34] M. Weber, A. Julbe, A. Ayril, P. Miele, M. Bechelany, Atomic layer deposition for  
571 membranes: Basics, challenges, and opportunities, Chemistry of Materials, 30 (2018) 7368-  
572 7390.

573 [35] O. Graniel, M. Weber, S. Balme, P. Miele, M. Bechelany, Atomic layer deposition for  
574 biosensing applications, Biosensors and Bioelectronics, (2018).

575 [36] M. Weber, J.-Y. Kim, J.-H. Lee, J.-H. Kim, I. Iatsunskyi, E. Coy, P. Miele, M.  
576 Bechelany, S.S. Kim, Highly Efficient Hydrogen Sensors Based on Pd Nanoparticles  
577 Supported on Boron Nitride Coated ZnO Nanowires, Journal of Materials Chemistry A,  
578 (2019).

579 [37] P.K. Gupta, S. Tiwari, Z.H. Khan, P.R. Solanki, Amino acid functionalized ZrO<sub>2</sub>  
580 nanoparticles decorated reduced graphene oxide based immunosensor, Journal of Materials  
581 Chemistry B, 5 (2017) 2019-2033.

582 [38] P.R. Solanki, M.K. Patel, M.A. Ali, B. Malhotra, A chitosan modified nickel oxide  
583 platform for biosensing applications, Journal of Materials Chemistry B, 3 (2015) 6698-6708.

584 [39] M.A. Ali, K. Kamil Reza, S. Srivastava, V.V. Agrawal, R. John, B.D. Malhotra, Lipid-  
585 lipid interactions in aminated reduced graphene oxide interface for biosensing application,  
586 Langmuir, 30 (2014) 4192-4201.

587 [40] Y. Xiang, M.B. Camarada, Y. Wen, H. Wu, J. Chen, M. Li, X. Liao, Simple  
588 voltammetric analyses of ochratoxin A in food samples using highly-stable and anti-fouling  
589 black phosphorene nanosensor, Electrochimica Acta, 282 (2018) 490-498.

590 [41] G. Zhang, Z. Liu, L. Fan, Y. Guo, Electrochemical prostate specific antigen aptasensor  
591 based on hemin functionalized graphene-conjugated palladium nanocomposites,  
592 Microchimica Acta, 185 (2018) 159.

593 [42] A.-E. Radi, X. Munoz-Berbel, V. Lates, J.-L. Marty, Label-free impedimetric  
594 immunosensor for sensitive detection of ochratoxin A, Biosensors and Bioelectronics, 24  
595 (2009) 1888-1892.

596 [43] F. Conzuelo, M. Gamella, S. Campuzano, D.G. Pinacho, A.J. Reviejo, M.P. Marco, J.M.  
597 Pingarrón, Disposable and integrated amperometric immunosensor for direct determination of  
598 sulfonamide antibiotics in milk, Biosensors and Bioelectronics, 36 (2012) 81-88.

599 [44] G. Yang, D. Chen, P. Lv, X. Kong, Y. Sun, Z. Wang, Z. Yuan, H. Liu, J. Yang, Core-  
600 shell Au-Pd nanoparticles as cathode catalysts for microbial fuel cell applications, Scientific  
601 reports, 6 (2016) 35252.

602 [45] S. Siddiqui, Z. Dai, C.J. Stavis, H. Zeng, N. Moldovan, R.J. Hamers, J.A. Carlisle, P.U.  
603 Arumugam, A quantitative study of detection mechanism of a label-free impedance biosensor  
604 using ultrananocrystalline diamond microelectrode array, Biosensors and Bioelectronics, 35  
605 (2012) 284-290.

606 [46] C. Zhou, D. Liu, L. Xu, Q. Li, J. Song, S. Xu, R. Xing, H. Song, A sensitive label-free  
607 amperometric immunosensor for alpha-fetoprotein based on gold nanorods with different  
608 aspect ratio, Scientific reports, 5 (2015) 9939.

609 [47] Y.S. Kim, J.H. Niazi, M.B. Gu, Specific detection of oxytetracycline using DNA  
610 aptamer-immobilized interdigitated array electrode chip, Analytica Chimica Acta, 634 (2009)  
611 250-254.

- 612 [48] L. Zhou, D.-J. Li, L. Gai, J.-P. Wang, Y.-B. Li, Electrochemical aptasensor for the  
613 detection of tetracycline with multi-walled carbon nanotubes amplification, *Sensors and*  
614 *Actuators B: chemical*, 162 (2012) 201-208.
- 615 [49] A. Kaushik, P.R. Solanki, A.A. Ansari, S. Ahmad, B.D. Malhotra, A nanostructured  
616 cerium oxide film-based immunosensor for mycotoxin detection, *Nanotechnology*, 20 (2009)  
617 055105.
- 618 [50] Q. Li, L. Zeng, J. Wang, D. Tang, B. Liu, G. Chen, M. Wei, Magnetic mesoporous  
619 organic– inorganic NiCo<sub>2</sub>O<sub>4</sub> hybrid nanomaterials for electrochemical immunosensors, *ACS*  
620 *applied materials & interfaces*, 3 (2011) 1366-1373.

621